Samuel L. Zelinka, Sophie-Charlotte Gleber, Stefan Vogt, Gabriela M. Rodríguez López and Joseph E. Jakes*

# Threshold for ion movements in wood cell walls below fiber saturation observed by X-ray fluorescence microscopy (XFM)

**Abstract**: Diffusion of chemicals and ions through the wood cell wall plays an important role in wood damage mechanisms. In the present work, free diffusion of ions through wood secondary walls and middle lamellae has been investigated as a function of moisture content (MC) and anatomical direction. Various ions (K, Cl, Zn, Cu) were injected into selected regions of 2 μm thick wood sections with a microinjector and then the ion distribution was mapped by means of X-ray fluorescence microscopy with submicron spatial resolution. The MC of the wood was controlled *in situ* by means of climatic chamber with controlled relative humidity (RH). For all ions investigated, there was a threshold RH below which the concentration profiles did not change. The threshold RH depended upon ionic species, cell wall layer, and wood anatomical orientation. Above the threshold RH, differences in mobility among ions were observed and the mobility depended upon anatomical direction and cell wall layer. These observations support a recently proposed percolation model of electrical conduction in wood. The results contribute to understanding the mechanisms of fungal decay and fastener corrosion that occur below the fiber saturation point.

**Keywords:** ionic conduction, micro X-ray fluorescence, percolation, wood anatomy, wood-moisture relations

DOI 10.1515/hf-2014-0138
Received April 29, 2014; accepted September 17, 2014; previously published online October 16, 2014

***Corresponding author: Joseph E. Jakes,** Forest Biopolymers Science and Engineering, USDA Forest Service, Forest Products Laboratory, One Gifford Pinchot Drive, Madison, WI 53726, USA, e-mail: jjakes@fs.fed.us
**Samuel L. Zelinka and Gabriela M. Rodríguez López:** Durability and Wood Protection Research, USDA Forest Service, Forest Products Laboratory, One Gifford Pinchot Drive, Madison, WI 53726, USA
**Sophie-Charlotte Gleber and Stefan Vogt:** Argonne National Laboratory, X-ray Science Division, 9700 South Cass Avenue, Argonne, IL 60439, USA

## Introduction

Moisture is the root cause of nearly all wood failures. Wood decay, mold growth, and fastener corrosion occur only when moisture is in abundance. Fluctuations in moisture content (MC) of wood cause large internal stresses, which lead to dimensional instability, warping, and splitting (checking) of the wood. Traditionally, water is believed to exist in one of two states in wood: "bound water", where water molecules are hydrogen bonded with cell wall polymers, or "free water", where water behaves similarly to bulk water and exists in void space within the wood structure (Stamm 1971; Berry and Roderick 2005). The fiber saturation point (FSP) would seem a logical threshold for chemical transport through wood because free water would be able to solvate ions or other chemicals. However, the thresholds for these damage mechanisms are much lower than the FSP, ranging between 15% and 25% MC (Griffin 1977; Baker 1988; Viitanen and Paajanen 1988; Dennis et al. 1995; Short and Dennis 1997; Carll and Highley 1999; Wang and Morris 2010; Jakes et al. 2013).

Recently, Jakes et al. (2013) proposed that damage mechanisms and chemical transport below the FSP are related to changes in the hemicelluloses with MC. As the cell wall absorbs moisture from the environment, local regions of hemicelluloses soften through a glass transition. The number and size of the softened regions increase with increasing MC until finally a percolating network of softened hemicelluloses form diffusion channels that transport ions and other chemicals. At room temperature, the hemicelluloses pass through their glass transition between 60% and 80% relative humidity (RH) (Cousins 1978; Kelley et al. 1987; Olsson and Salmen 2004), which corresponds to approximately 15% MC and the lower MC threshold observed for damage. This MC is also close to the percolation threshold for ionic conduction found by Zelinka et al. (2008).

The only measurements to examine ion movement as a function of MC in wood were conducted by Lin in the 1960s and, to our knowledge, were never published beyond his PhD dissertation (Lin 1965). Lin implanted radioactive ions

into blocks of wood, stacked the blocks of wood together, applied a bias voltage, and measured the net change in radioactivity in each block. The key findings of Lin are plotted in Figure 1. For low MCs, the ratio of counting rates before and after the experiment was the same, indicating no net movement of ions. At high MCs, the ratio of counts before and after the voltage showed fewer Na-22 and more I-131 in the block nearest the cathode. The lowest MC showing net migration of tagged ions appears to be 16%.

While the data in Figure 1 suggest a 16% MC threshold for ionic conduction, the actual threshold could be vastly different depending on the measurement's details. Migration was observed only by a change in radioactivity of an individual block. Because the blocks were 3 mm thick, ions needed to migrate from one tracheid to another to even be observed. Furthermore, developing a mechanistic interpretation of how the ions moved through the wood is impossible because only net migration of charge was studied. The measurements are also limited in MC space because only four MCs (5%, 13%, 16%, and 28%) were tested.

This paper explores the MC threshold for ion movement in wood by using synchrotron-based X-ray fluorescence microscopy (XFM) to observe the effects of MC, ion species, and anatomic direction on ion mobility in secondary cell walls (S2) and middle lamellae (ML) in loblolly pine (*Pinus taeda* L.). XFM allows the quantification of element concentration down to trace quantities at submicron spatial resolutions and it can therefore be used to differentiate diffusion in the S2 from ML. A custom-built climatic chamber and RH generator for the beamline allows for the MC of the samples to be changed *in situ*.

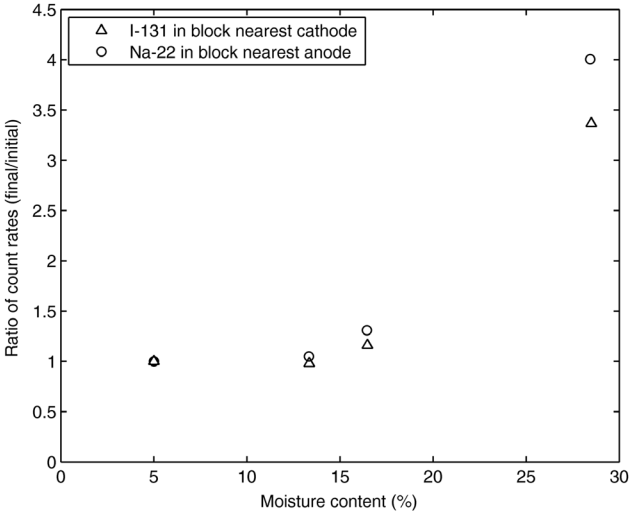


**Figure 1** Ionic conduction data of Lin (1965) after 5 h under an applied electric field. The y-axis effectively plots the ratio of the concentration of sodium/iodide ions before and after the measurement.

## Materials and methods

Wood sections (2 μm thick) were cut from latewood loblolly pine (*Pinus taeda*) with a diamond knife in combination with a Sorvall (Norwalk, CT, USA) MT-2 ultramicrotome. The knife boat was filled with deionized water. Rectangular sections (100–300 μm wide and 2–3 mm long) of both transverse (Tr) and tangential-longitudinal (L) orientations were prepared. The sections were lifted from the water and held flat while drying. The dried sections were then clamped spanning the hole of a copper StrateTek™ 1/1 mm double folding TEM grid (Ted Pella Inc., Redding, CA, USA).

Ions were injected into small regions of the wood sections by means of borosilicate glass micropipettes made by a P-2000 laser pipette puller (Sutter, Novato, CA, USA). The pipettes were connected to a XenoWorks™ Digital Microinjector (Sutter, Novato, CA, USA), which allowed for generation of small (<100 μm in diameter) droplets of KCl, $CuSO_4$ and $ZnSO_4$ saturated salt solutions. Filling the pipettes and ejecting the salt solution onto the dry wood was challenging because of the small pipette openings and the large surface tension of the salt solutions. Surface tension was lowered by diluting the salt solutions to 50% (by vol.) ethanol. Pipettes were partially filled from the back end by a hand syringe, which left an air bubble near the tip. The pipette was then connected to the microinjector and immersed in the salt solution. The pressure was then cycled through pressure and vacuum until the air bubble disappeared.

The micropipette and droplet position was observed with an inverted microscope (Leica, Wetzlar, Germany) and positioned with a micromanipulator (Sutter, Novato, CA, USA). The fixed dry wood section was placed on a microscope slide and observed at 100× magnification. After positioning the pipette with the micromanipulator, 1.0–1.2 kPa of pressure was applied through the microinjector in continuous mode until a droplet was visible in the microscope, at which point the injection was stopped and the droplet imaged so that the injected area could be located in the XFM experiment (Figure 2). Because of the heat produced by the light microscope, the droplets

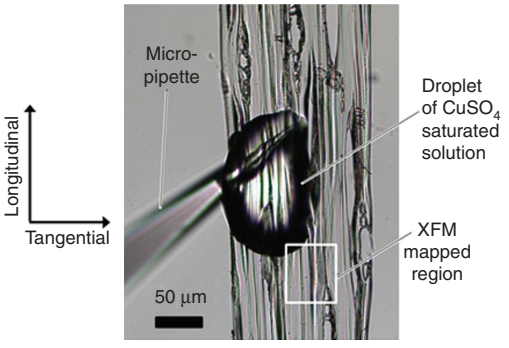


**Figure 2** Optical microscopy image of the implantation process on a 2 μm thick L section of latewood loblolly pine; note that most droplets were smaller in size than the one shown. The region mapped with X-ray fluorescence microscopy in Figure 3a is indicated with a white box.

dried almost instantaneously, resulting in a steep concentration gradient around the droplet-positioning place.

High-resolution XFM at beamline 2-ID-E at the Advanced Photon Source at Argonne National Laboratory (Argonne, IL, USA) was applied. The RH was controlled in a custom RH chamber during XFM. The RH chamber (constructed of an Al frame covered by Kapton™ film; DuPont, Wilmington, DE, USA) was integrated into the beamline and had an inlet and outlet hose for continuous purging with a gas (in this case $N_2$). The RH of $N_2$ was controlled with a HumiSys™ RH generator (Instruquest, Coconut Creek, FL, USA) capable of an output of 2 l $min^{-1}$. The temperature (31°C–33°C) and RH inside the chamber was continuously monitored by a Sensirion (Staefa, Switzerland) SHT1x sensor. In some experiments, the humidity was maintained throughout the time needed for collecting the XFM image (1–3 h); in other experiments, the specimen was conditioned for 10–30 min at higher RH and the XFM maps were collected under dry conditions. The incident X-ray beam energy was 10.2 keV, and spot size was approximately 0.8 μm in the horizontal and 0.5 μm in the vertical. Elemental maps were built in 0.3 μm step sizes with 5 ms dwell times at each step. Data analysis was carried out by the MAPS software package (Vogt 2003). In brief, the full spectra were fit to modified Gaussian peaks, the background was iteratively calculated and subtracted, and the results were compared to standard reference materials (RF4-100-S1749, AXO DRESDEN GmbH, Heidenau, Germany). A 3 by 3 median filter was applied to all XFM maps below.

## Results and discussion

XFM maps of implanted Cu ions in wood cell walls conditioned at different RH are shown in Figure 3. For the Cu experiments, the RH was maintained during the imaging. Also included at the top of Figure 3a and the left of Figure 3b are maps of Zn, a naturally occurring trace element in wood that has a higher concentration in the ML than the S2 (Saka and Goring 1983). The Zn map was useful for visualizing the ML, which appear as areas of higher Zn concentration. The S from the sulfate counterion did not have a strong signal in the XFM, but appeared to be similar to the Cu maps, as would be expected from charge neutrality arguments. The S maps are excluded to save space. For the L section, XFM maps were collected at 11 target RH conditions (50%–95%) and the first changes indicative of ion movements were observed in the 65% RH image (Figure 3a). However, an 80% RH spike occurred while the image was being taken, and therefore the threshold for initial ion movement could be between 65% and 80% RH. At higher RH levels, the Cu diffusion front continued to progress through both the S2 and ML at approximately the same rate with a higher concentration in the ML than the S2.

Ten different RH levels (40%–90%) were investigated for Cu ion movement in the Tr section. The first movement was observed after 70% RH conditioning, when a small finger of Cu was seen extending along a ML (see arrow in 70% RH image of Figure 3b). Because of a moisture fluctuation during the imaging, the actual threshold for ion movement could have been between 65% and 80% RH. As the RH increases, more diffusion through the interconnecting ML was observed (see arrow in 85% RH image of Figure 3b) in addition to increased concentrations in the S2 near the initial Cu concentration front. Three successive images were also collected at 90% RH as a time series (Figure 3c) showing extensive diffusion through the neighboring cells, with the diffusion front moving faster through the ML than the S2.

The results of the $ZnSO_4$ experiments are shown in Figure 4. In these measurements, specimens were preconditioned at the respective RH for 10 min, and imaged under dry air to minimize problems caused by fluctuations in the RH chamber during imaging. The L section was conditioned twice at 70% RH and then at four additional RH levels (75%–90%). Two fronts were visible: an extremely bright region of high concentration in the upper right-hand corner and a less bright region that was higher concentration than the naturally occurring Zn and initially extended approximately 20 μm out from the bright region. This less bright region was implanted Zn in the cell walls. The brighter region may have been a region of supersaturation or Zn residing at the surface. The first movement in the implanted Zn was observed between 85% and 90% RH. Further measurements were performed, where the RH was brought to 90% and held there for several hours during successive scans (Figure 4b). The less bright Zn concentration front moved downward in both the S2 and ML at approximately the same rate and it was observed to travel downward about 60 μm within 190 min. The brighter region did not move very far, but instead exhibited a coalescence of supersaturated regions, first visible in the image taken at 190 min, and the front remained in approximately the same place for the remainder of the experiments.

Figure 4c shows the concentration of implanted Zn ions as a function of position in the Tr section after 10 min preconditioning steps at target RHs between 50% and 85%, with an additional 30 min conditioning at 85% RH. Transport was observed in the ML after conditioning at 74% RH, suggesting a threshold for Zn ion diffusion between 67% and 74% RH (see arrows in 67% and 74% RH images of Figure 4c). Although less obvious, small changes in the concentration of Zn in the S2 could also be observed. This could be most clearly observed in the second cell from the bottom in the leftmost row where there was a high concentration of Zn around the right side of the lumen at 50% RH, but at 74% RH and above this high concentration region

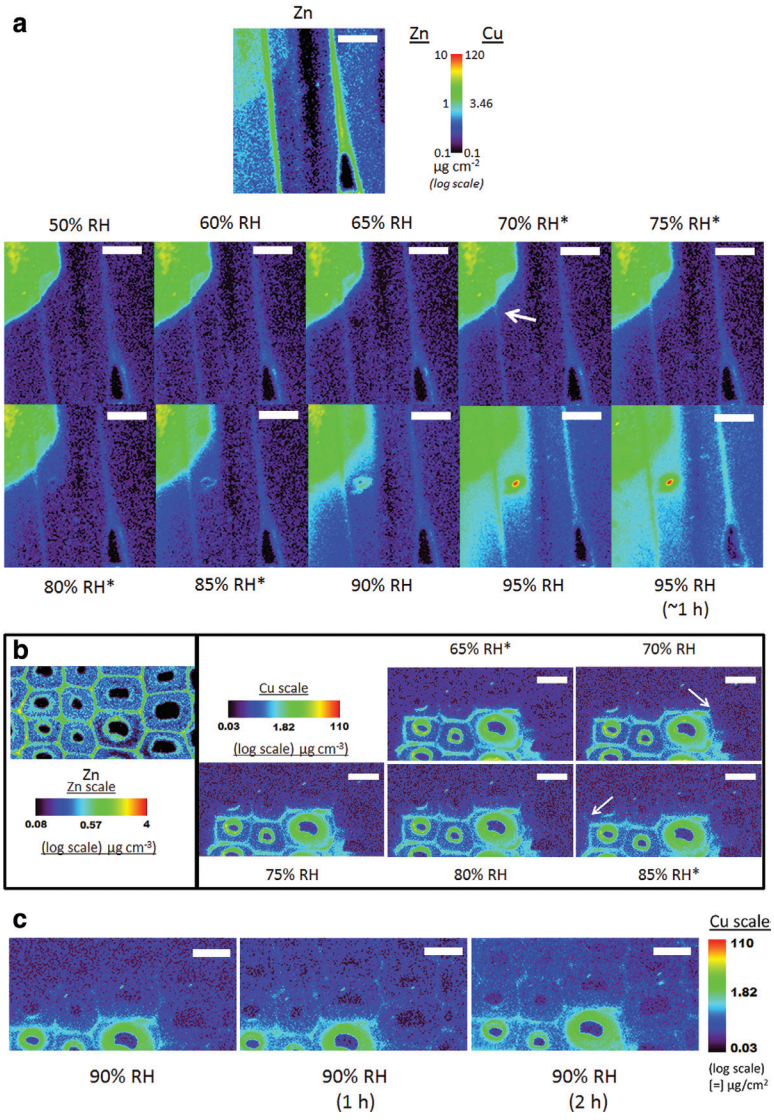


**Figure 3** X-ray fluorescence microscopy maps of Cu concentration as a function of relative humidity in the L (a) and Tr directions (b and c). The Zn maps are included to highlight the middle lamellae. Relative humidity (RH) values denoted by * experienced a spike in RH during the imaging. Scale bar=20 µm.

softened as Zn gradually diffused into the surrounding cell wall material.

The results of implanted KCl diffusion are presented in Figure 5. In contrast to the sulfate, the Cl could be clearly imaged with XFM, and these maps are included. For these experiments both the L and Tr sections were placed in the RH chamber at the same time and XFM maps were obtained after conditioning for 10 min at eight target RH conditions (40%–75%). The brightest regions were salt crystals on the section surfaces. In the L section (Figure 5a) diffusion of both implanted K and Cl was first observed in the 67% RH image, thus bounding the RH threshold for ion movement between 60% and 67% RH. As RH increases, both the K and Cl ion fronts move similar distances. However, in contrast to the Zn and Cu, both ions have lower concentrations in ML than the S2 as diffusion progresses, suggesting a lower diffusion coefficient in the ML for these ions.

Moisture-induced transport of K and Cl ions in the Tr orientation are shown in Figure 5b. Diffusion was first observed in both the ML and S2 after 67% RH conditioning, which bounded the RH threshold between 60% and 67% RH. In contrast to Zn and Cu, as RH increases, the K and Cl concentration fronts appeared to move faster through the S2 than the ML and the concentration in the ML was lower in the ML as diffusion progressed. These

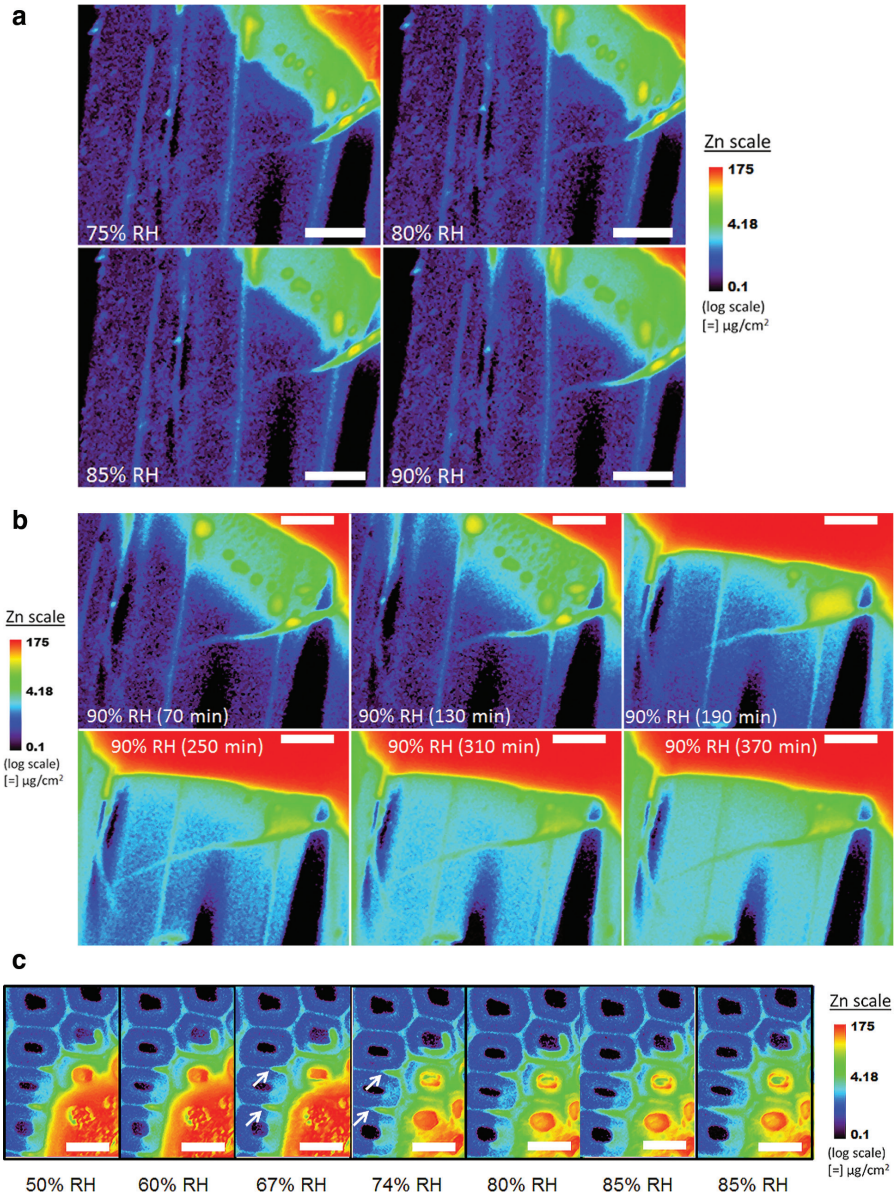


**Figure 4** Zn X-ray fluorescence microscopy maps as a function of relative humidity in the L (a and b) and Tr directions (c). Scale bar=20 µm.

observations support the observation from the L section that diffusion was slower in the ML than S2 for K and Cl.

A summary of the observed moisture thresholds for Cu, Zn, K, and Cl ion movements is given in Table 1. These ions were chosen because they are important in wood processes. The diffusion of Cu and Zn is important for fastener corrosion in treated wood (Zelinka and Stone 2011). K and Cl are two of the most common ions in wood, and their concentrations have a strong effect on electrical properties of wood (Simons et al. 1998; Zelinka et al. 2008). A potential concern is whether the observed ion transport is diffusion through the wood or flow across the section surface through salt deliquescence. Deliquescence is the process by which hygroscopic salts form a solution phase from moisture in the air when the activity of water in the vapor phase is less than one. At 25°C, KCl salt deliquesces at 84% RH (Greenspan 1977) and $ZnSO_4$ and $CuSO_4$ salts deliquesce at 90% RH and 98% RH, respectively (Greenland and Hayes 1978). In experiments not shown, deliquescence of a KCl salt was observed above 84% RH. The deliquescence was obvious because large regions with concentration nearly as high as the original salt crystals appeared up to 100 µm from the original salt crystals. Presumably, the KCl deliquesced

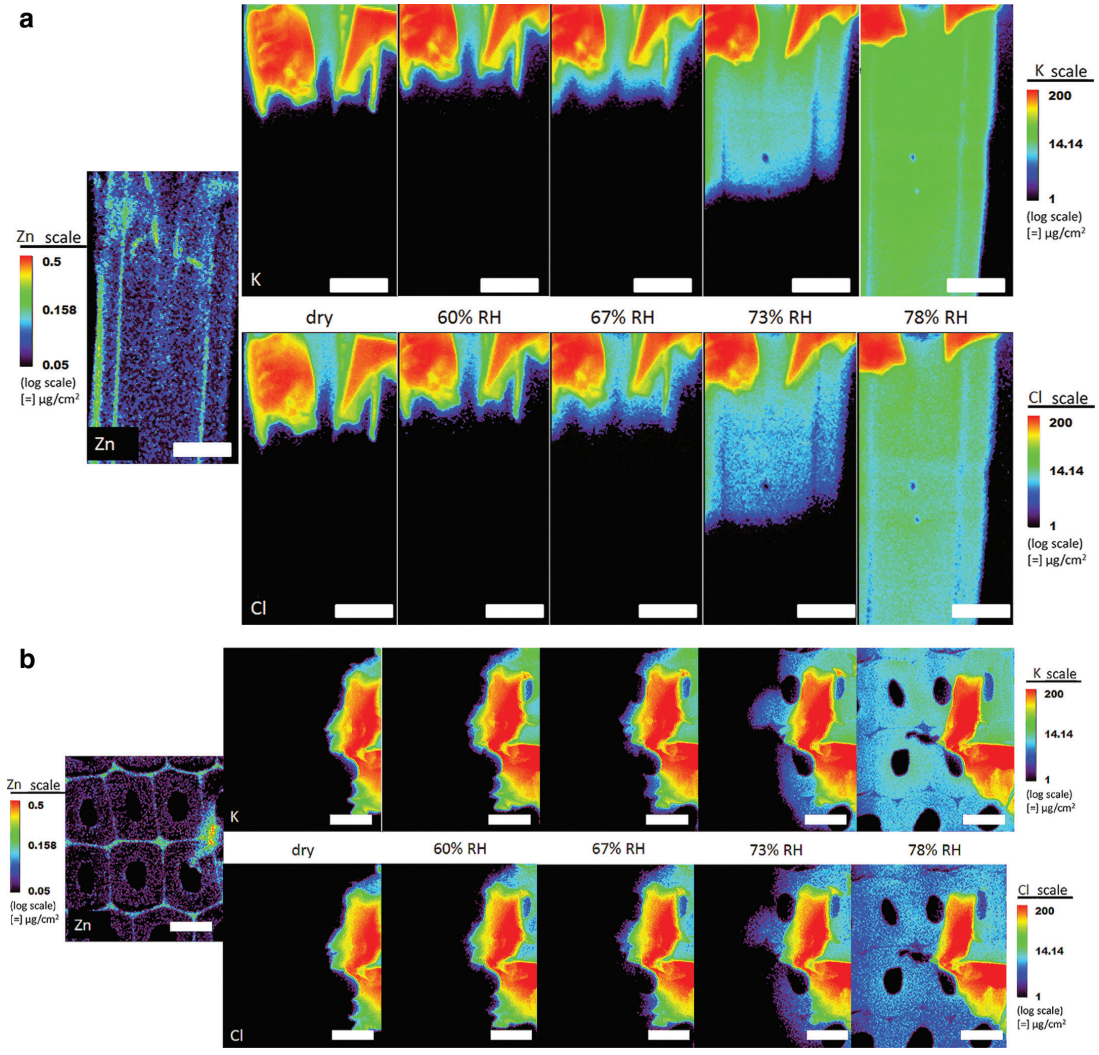


**Figure 5** X-ray fluorescence microscopy maps of concentration of Cl (bottom) and K (top) ions as a function of relative humidity in the L (a) and Tr directions (b).
Scale bar=20 µm.

**Table 1** Summary of observed relative humidity (RH) ranges for the onset of ion diffusion.

| Ion | Orientation | RH for diffusion onset (%) | RH during imaging | Figure |
|---|---|---|---|---|
| Cu | L | 65–80 | @RH | 3 |
| Cu | Tr | 65–80 | @RH | 3 |
| Zn | L | 85–90 | Dry | 4 |
| Zn | Tr | 67–74 | Dry | 4 |
| K | L | 60–67 | Dry | 5 |
| K | Tr | 60–67 | Dry | 5 |
| Cl | L | 60–67 | Dry | 5 |
| Cl | Tr | 60–67 | Dry | 5 |

"@RH" means the RH was maintained during the imaging and "Dry" means the specimen was preconditioned for 10 min before imaging under dry $N_2$. L, longitudinal; Tr, transversal.

and flowed across the sample surface. The observed RH ranges for K and Cl transport were 60%–65% RH, much lower than the KCl 84% RH deliquescence point, and therefore, the observed transport onset was diffusion through the wood and not deliquescence. Similarly, the observed RH ranges for Cu transport and Zn transport in the Tr section were much lower than their respective salt deliquescence RHs. However, the observed 85%–90% RH range for Zn transport in the L section was approaching the 90% $ZnSO_4$ deliquescence RH. The movement appeared to be diffusion through the wood because the observed movement was similar to the movement observed for other ions far below their deliquescence points, and not flow of high concentration regions over the surface.

Insights to how ions move through wood cell walls can be gained from the XFM maps above the onset threshold RH for diffusion. Ion mobility was dependent on the ion type. Movements of Zn, K, and Cl ions were the easiest to compare because they were all tested with the same well-defined 10 min preconditioning steps. In both L and Tr orientations, K and Cl concentration fronts moved faster than that of Zn for a given RH. Diffusion fluxes of K and Cl appeared to be higher than that of Zn, but differences in initial concentrations precluded a direct comparison.

In addition to being ion dependent, the mobility of ions also depended upon RH, orientation, and cell wall layer. For all ions, the rate of diffusion increased with increasing RH. Concentration fronts generally moved faster in the L direction than in the Tr direction, as was readily observed comparing the distance traveled by K and Cl fronts during the 10 min 70% RH conditioning steps in Figure 5. This was not surprising, because in bulk wood specimens, electrical conductivity of wood is known to be roughly twice as fast in the L direction as in the Tr direction (Glass and Zelinka 2010). Interestingly, different ions were transported differently in the S2 and ML. These differences were most easily observed in the Tr sections. Initial concentrations of Cu and Zn were higher in the ML and Cu and Zn appeared to transport faster through the ML than in the S2.

Results of the diffusion experiments performed in this paper were consistent with a mechanism where hemicelluloses softening forms diffusion channels, resulting in percolative electrical properties. The ions embedded in the wood did not move until a threshold MC was reached, which occurred between 60% and 90% RH, depending on the ion, cell wall layer, and orientation. Correspondingly, softening of hemicelluloses has been observed at room temperature in the range of 60%–80% RH (Cousins 1978; Kelley et al. 1987; Olsson and Salmen 2004). However, in contrast to the percolation model, which predicts a conductivity of zero below the percolation threshold, wood actually exhibits a small but finite conductivity below the percolation threshold that could not previously be explained. These XFM measurements show that the diffusion threshold depends upon ionic species, and instead of a single percolation threshold, there may be different thresholds for different ions, which could explain the conductivity below the percolation threshold of 16% MC suggested by Zelinka et al. (2008).

Thresholds for ion movement presented in this paper have implications for wood damage mechanisms and biorefinery pretreatments. Wood damage mechanisms such as fungal decay and fastener corrosion also occur below FSP, and Jakes et al. (2013) hypothesized that the underlying mechanism responsible for the onset of these wood degradative processes is controlled by the onset of chemical transport through wood cell walls. If true, wood treatments that raise the glass transition of hemicelluloses should be effective in protecting forest products from decay and minimizing fastener corrosion. Similarly, transition metal catalysts are being proposed for biorefinery pretreatments (Wei et al. 2011; Yu et al. 2011). Understanding and quantifying diffusion of the metal through cell walls is critical to improving these processes. Further exploration of subcellular transport and mechanical properties as a function of MC in both unmodified and modified wood known to provide protection would further substantiate the relationship between softening of hemicelluloses, onset of chemical transport, and the role chemical transport plays in wood degradation and biorefinery pretreatments.

## Conclusions

Diffusion of Zn, Cu, K, and Cl ions implanted into wood cell walls was observed by XFM mapping as a function of MC and anatomical orientation. The high spatial resolution of XFM allowed differentiation of ions in the ML and S2. In all ions studied, a threshold MC was identified below which ion transport did not occur. The threshold for ion transport depended upon ion species, cell wall layer, and wood anatomical direction. Observed thresholds were as low as 60% RH for K and Cl ions and as high as 90% RH for Zn ions. Above the threshold, ion mobility could also be observed to depend on the type of ion, cell wall layer, and anatomical orientation. The threshold for ion movement in wood, confirmed in this paper, has implications for electrical properties in wood and sets a lower MC bound on wood degradation processes that require ion movement, such as fastener corrosion and wood decay fungi. This mechanism for ion transport below FSP is consistent with the mechanism of softened hemicelluloses previously proposed.

**Acknowledgments:** JEJ and SLZ acknowledge funding from 2011 and 2010 USDA PECASE Awards, respectively. GMR acknowledges the SURE-REU program at UW-Madison for support to conduct research during summer 2013. The use of Advanced Photon Source facilities was supported by the US Department of Energy, Basic Energy Sciences, Office of Science, under contract number W-31-109-Eng-38. The authors acknowledge the machine shop at the Forest Products Laboratory for construction of the in situ relative humidity chamber.

## References


Baker, A.J. (1988) Corrosion of metals in preservative-treated wood. In: Wood Protection Techniques and the Use of Treated Wood in Construction. Ed. Hamel, M. Forest Products Society, Madison, WI. pp. 99–101.

Berry, S.L., Roderick, M.L. (2005) Plant-water relations and the fibre saturation point. N. Phytol. 168:25–37.

Carll, C., Highley, T.L. (1999) Decay of wood and wood-based products above ground in buildings. J. Test. Eval. 27:150–158.

Cousins, W. (1978) Young's modulus of hemicellulose as related to moisture content. Wood Sci. Technol. 12:161–167.

Dennis, J.K., Zou, C., Short, N.R. (1995) Corrosion behaviour of zinc and zinc alloy coated steel in preservative treated timber. Trans. Inst. Met. Finish. 75:96–101.

Glass, S.V., Zelinka, S.L. (2010) Moisture relations and physical properties of wood. In: Wood Handbook: Wood as an Engineering Material. Ed. Ross, R.J. GTR-190. U.S. Department of Agriculture, Forest Service, Forest Products Laboratory, Madison, WI. pp. 4.1–4.19.

Greenland, D.J., Hayes, M.H.B. (1978) The chemsitry of soil constituents. John Wiley & Sons, Chichester.

Greenspan, L. (1977) Humidity fixed points of binary saturated aqueous solutions. J. Res. Natl. Stand. Sec. A. 81A:89–96

Griffin, D. (1977) Water potential and wood-decay fungi. Annu. Ref. Phytopathol. 15:319–329.

Jakes, J.E., Plaza, N., Stone, D.S., Hunt, C.G., Glass, S.V., Zelinka, S.L. (2013) Mechanism of transport through wood cell wall polymers. J. For. Prod. Ind. 2:10–13.

Kelley, S.S., Rials, T.G., Glasser, W.G. (1987) Relaxation behaviour of the amorphous components of wood. J. Mater. Sci. 22:617–624.

Lin, R.T. A study of electrical conduction in wood. State College of Forestry at Syracuse University. Syracuse, NY, 1965.

Olsson, A.M., Salmen, L. (2004) The softening behavior of hemicelluloses related to moisture. In: Hemicelluloses: Science and Technology. Eds. Gatenholm, P., Tenkanen, M., vol. 864. ACS Publications, Washington, DC. pp. 184–197.

Saka, S., Goring, D.A.I. (1983) The distribution of inorganic constituents in black spruce wood as determined by TEM-EDXA. J. Jpn. Wood Res. Soc. 29:648–656.

Short, N.R., Dennis, J.K. (1997) Corrosion resistance of zinc-alloy coated steel in construction industry environments. Trans. Inst. Met. Finish. 75:47–52.

Simons, P.J., Spiro, M., Levy, J.F. (1998) Electrical transport of endogenous mineral ions in green sapwood of *Pinus sylvestris L.* (Scots pine). Wood Sci. Tech. 32:403–410.

Stamm, A.J. (1971) Review of nine methods for determining the fiber saturation points of wood and wood products. Wood Sci. 4:114–128.

Viitanen, H., Paajanen, L. (1988) The critical moisture and temperature conditions for the growth of some mould fungi and the brown rot fungus *Coniophora puteana* on wood. International Research Group on Wood Protection, Madrid. IRG/WP 1369.

Vogt, S. (2003) MAPS: A set of software tools for analysis and visualization of 3D X-ray fluorescence data sets. J. Phys. IV. 104:635–638.

Wang, J., Morris, P.I. (2010) A review on conditions for decay initiation and progression. International Research Group on Wood Protection, Biarritz. IRG/WP 10-20444.

Wei, H., Donohoe, B.S., Vinzant, T.B., Ciesielski, P.N., Wang, W., Gedvilas, L.M., Zeng, Y., Johnson, D.K., Ding, S.-Y., Himmel, M.E. (2011) Elucidating the role of ferrous ion co-catalyst in enhancing dilute acid pretreatment of lignocellulosic biomass. Biotechnol. Biofuel. 4:48.

Yu, Q., Zhuang, X., Yuan, Z., Qi, W., Wang, Q., Tan, X. (2011) The effect of metal salts on the decomposition of sweet sorghum bagasse in flow-through liquid hot water. Bioresour. Technol. 102:3445–3450.

Zelinka, S.L., Stone, D.S. (2011) Corrosion of metals in wood: comparing the results of a rapid test method with long-term exposure tests across six wood treatments. Corros. Sci. 53:1708–1714.

Zelinka, S., Glass, S., Stone, D. (2008) A percolation model for electrical conduction in wood with implications for wood-water relations. Wood Fib. Sci. 40:544–552.